Residual stress variation in SiCf/SiC composite during heat treatment and its effects on mechanical behavior

Xiaowu Chen (xwchen@mail.sic.ac.cn)
Shanghai Institute of Ceramics Chinese Academy of Sciences https://orcid.org/0000-0002-8923-2937
Guofeng Cheng
Shanghai Institute of Ceramics Chinese Academy of Sciences
Junmin Zhang
Shanghai Institute of Ceramics Chinese Academy of Sciences
Feiyu Guo
Shanghai Institute of Ceramics Chinese Academy of Sciences
Haijun Zhou
Shanghai Institute of Ceramics Chinese Academy of Sciences
Chunjin Liao
Shanghai Institute of Ceramics Chinese Academy of Sciences
Hongda Wang
Shanghai Institute of Ceramics Chinese Academy of Sciences
Xiangyu Zhang
Shanghai Institute of Ceramics Chinese Academy of Sciences
Shaoming Dong
Shanghai Institute of Ceramics Chinese Academy of Sciences

Research Article

Keywords: Residual stress, Nano-powder infiltration and transient eutectoid (NITE), Raman spectroscopy, Mechanical properties.

Posted Date: June 3rd, 2020

DOI: https://doi.org/10.21203/rs.3.rs-20936/v2

Version of Record: A version of this preprint was published at Journal of Advanced Ceramics on July 25th, 2020. See the published version at https://doi.org/10.1007/s40145-020-0395-4.

Abstract

Residual stress originated from thermal expansion mismatch determines the mechanical properties of ceramic matrix composites (CMCs). Here, continuous SiC fiber reinforced SiC matrix (SiC_f/SiC) composites were fabricated by nano-infiltration and transient eutectic-phase (NITE) method, and the residual stress of the composites was investigated using high-temperature Raman spectrometer. With temperature increasing from room temperature to 1400℃, the residual stresses of the matrix and the fiber decrease from 1.29 GPa to 0.62 GPa and from 0.84 GPa to 0.55 GPa in compression respectively, while that of the interphase decreases from 0.16 GPa to 0.10 GPa in tension. The variation of residual stress shows little effect in the tensile strength of the composites, while causes a slight decrease in the tensile strain. The suppression of fiber/matrix debonding and fiber pulling-out caused by the residual stress reduction in the interphase is responsible for the decreasing tensile strain. This work can open up new alternatives for residual stress analysis in CMCs.

1. Introduction

Ceramic matrix composites (CMCs), possessing excellent mechanical properties and corrosion resistance at high temperature, show great advantage over superalloys in aerospace applications. The advantage, however, may be compromised due to cracks pre-existed in the composites or induced by external service environment. The formation of cracks is dependent on various factors, of which residual stress plays an important role [1,2]. For CMCs materials, which are prepared and served in high temperature (≥1000℃) conditions, residual stress is inevitably formed due to the thermal expansion mismatch of the constituent phases. To maximize the vast benefits of CMCs, it is quite necessary to determinate and control the residual stress.

There are several methods to measure residual stress, including X-ray diffraction [3,4], neutron diffraction [5,6], Raman spectroscopy [7,8] and mechanical loading [9,10]. Both X-ray and neutron diffraction methods obtain residual stress by measuring average thermal strain. However, interpretation of the data obtained from diffraction experiments can be very difficult when there are crystallographic defects (dislocation, stacking faults, etc.) in the sample. Among them, Raman spectroscopy can directly measure residual stress without analyzing the intermediate data, and has attracted increasing attention since it was first reported in 1970s [11]. Wing *et al*. [12] adopted Raman spectroscopy to investigate the residual stress in reaction-bonded SiC, and measured residual compressive stress as high as ~2.0 GPa in the silicon phase and residual tensile stress as high as ~2.3 GPa in the SiC phase, both of which are higher than those calculated from thermal expansion mismatch. The high residual stresses are attributed to the volumetric change of the unreacted silicon during crystallization. John *et al*. [13] studied the effects of SiC content on the residual stress of Al_2O_3/SiC composite through Raman technique. Residual compressive stress of the SiC phase decreases linearly from 2.0 GPa to 1.6 GPa as the SiC volume content increases from 12% to 30%. In addition, Raman spectroscopy has also been widely used to measure residual stress in ZrB_2-SiC [14], B_4C-ZrB_2 [15], C_f/SiC [16] composites, indicating its great universality in residual stress analysis.

SiC_f/SiC (continuous SiC fiber reinforced SiC matrix composite) is one of the most important CMCs due to its huge application prospects in hot sections of aeroengine. Compared with other CMCs (such as C_f/SiC and C_f/Si_3N_4), SiC_f/SiC shows relative lower residual stress due to the smaller difference of chemical compositions and microstructures between the constituent phases. Still, the residual stress in SiC_f/SiC cannot be ignored considering the high preparation/service temperatures and the anisotropic fiber orientation. Kollins *et al*. [17] measured the residual stress in melt infiltrated SiC_f/SiC through Raman method and found that all the constituent phases show rather different residual stresses. Residual stress of the free silicon is ~2 GPa in compression, while residual stresses of the matrix and the fiber are ~1.45 GPa and ~05-0.7 GPa in tension, respectively. Knauf *et al*. [18] studied the residual stress distribution in slurry melt-infiltrated SiC_f/SiC and found the residual stress of the intratow silicon is ~180 MPa in compression, while the compressive stress of the matrix is ~300 MPa. Furthermore, heat treatment at 1300℃ for 1 hour in the composite was found to have little influence on the residual stress distribution [19]. In fact, the final state of residual stress during heat treatment is closely related with the cooling rate. This may cause uncertainty in the analysis of residual stress as different cooling rates may lead to different residual stresses. In order to investigate the residual stress precisely, in-situ measurement (such as high-temperature Raman spectroscopy) independent of cooling conditions should be utilized.

In this study, the residual stress of SiC_f/SiC prepared by nano-infiltration and transient eutectic-phase (NITE) method was investigated using high-temperature Raman spectroscopy. As the SiC_f/SiC composites were formed through a high temperature and pressure sintering process, post-heating treatments were performed to adjust the residual stress. The variation of residual stress during the treatments were in-situ measured and the effects of treatment temperature on the residual stress were discussed. Besides, the effects of residual stress on the mechanical properties (tensile strength, fracture mode, *etc*.) were also revealed. This study can offer new insight for residual stress determination and important guidance for residual stress control in CMCs.

2. Experimental Procedure

2.1 Material preparation

The SiC_f/SiC composites were prepared by a nano-infiltration and transient eutectic-phase (NITE) process, which is specified in previous literature [20]. Firstly, continuous SiC fibers (Cansas3303, Fujian Leaoasia New Material LTD, Quanzhou, China) were aligned to form unidirectional fiber cloth (70 mm×70 mm), and then coated with BN interphase (~500 nm thick) via chemical vapor deposition (CVD) method using BCl_3 and NH_3 as the source gas. The CVD temperature was 900℃ and the pressure was 1.2 kPa. Subsequently, the fiber cloths were impregnated with a SiC slurry, which mainly consisted of SiC powder (~0.7μm, Weifang Kaihua Silicon Carbide Micropowder LTD, Weifang, China), 5 wt% binder (PVB) and 10 wt% sintering additive (SiO_2-40%Al_2O_3-20%Y_2O_3). The impregnated fiber cloths were stacked together and cured at 120℃ under pressure of 5MPa. Finally, SiC_f/SiC composites were obtained by pyrolyzing the

cured preform at 900℃ for 1.5 h and subsequent sintering at 1600℃ for 1 h under pressure of 20MPa. The volume fraction of fiber in the composites is ~25% and the density of composites is ~2.84 g•cm^{-3}.

2.2 Residual stress determination

The fundamental for residual stress determination using Raman spectrometer is that residual stress (σ_r) depends closely on Raman peak shift (dλ), and the mathematical relationship between them is linear (σ_r = C × dλ) [21,22]. This makes the calculation of residual stress directly based on the Raman peak shift. Raman spectra of the SiC_f/SiC samples were collected using a Renishaw Raman Spectrometer (532 nm laser, 20 mW, model inVia, Blue Scientific Limited, Cambridge, UK), which is equipped with inbuilt heating unit. Before the residual stress measurement, the SiC_f/SiC slices (4 mm×4 mm×1 mm) were polished using diamond polishing compound of 3 μm and 1 μm to eliminate the measurement error caused by surface roughness. The measurement temperature range was set from room temperature to 1400℃, with a heating rate of 15℃/min. As the temperature reached to the plateau, extra holding time of 5 min was required before the Raman data collection. Also, at least six measuring times were required for every measurement to ensure repeatability. To calculate the Raman peak shift, characteristic stress-free peaks at 796 cm^{-1}, 1365 cm^{-1} and 1585 cm^{-1} were chosen as the references for the SiC matrix, BN interphase and SiC fiber, respectively. All the measurements were performed in high-pure argon (99.9997%) atmosphere.

2.3 Mechanical test and microstructure characterization

Tensile tests of the SiC_f/SiC composites were conducted on a mechanical testing machine (DDL20, Changchun Research Institute for Mechanical Science Co. Ltd, Changchun, China) at room temperature, with a span of 45 mm and a loading rate of 0.5mm/min (ASTM C1275). For each group of the composites, at least five samples of 5 mm × 12 mm × 60 mm in dimension were used for the tests, and the reported mechanical strengths were the averaged values. Phase composition of the composites was analyzed using a Rigaku D/max X-ray diffractometer (Rigaku Corporation, Kyoto, Japan) with monochromated Cu-Kα radiation. Cross-sectional and fracture morphologies of the composites were observed using a SU8220 field emission scanning electron microscope (Hitachi, Tokyo, Japan). The energy dispersive spectra of the composites were collected using an energy-dispersive spectrometer (EDS, Inca energy, Oxford, UK).

3. Results And Discussion

The cross-sectional morphologies of the SiC_f/SiC composites indicate that both the fiber and the interphase remain intact (Fig. 1). Besides, the SiC matrix is almost distributed homogeneously and densely between the fibers. These structure features are quite different from the SiC_f/SiC composites derived from polymer infiltration and pyrolysis (PIP) [23,24] and chemical vapor infiltration (CVI) [25,26], which show rather porous structures due to the restricted mass transfer during the fabrication process. The high temperature/pressure of NITE process adopted in present study contributes to the highly dense

structure, but can also lead to high residual stress in the composites. It should be reminded here that the BN interphase is unobserved in the XRD patterns (Fig. 1d), which is mainly attributed to its low volume content (~3.3 vol%). In addition, the SiC phase exhibits two sets of crystal parameters that have subtle difference, which may correspond to the SiC fiber and the SiC matrix respectively. The energy dispersive spectra (Fig. 2) of the composites confirm that the BN interphase is mainly composed of B and N elements. The interphase almost remains unreacted with the fiber and the matrix. This makes it feasible to measure residual stress in the interphase using Raman spectroscopy.

Relaxation of residual stress is usually realized via annealing process, during which the material is heated at temperature lower than the preparation temperature. With the aid of thermal excitation, the crystallographic microstructures (grain size, grain boundary, grain orientation, etc.) can achieve significant transformation through atom diffusion or defect annihilation. Accompanying with the microstructure transformation, residual stress also experiences remarkable relaxation. Here, residual stress variation of the SiC_f/SiC composites was in-situ investigated by a high-temperature Raman Spectrometer, and the Raman spectra at RT~1400℃ are shown in Fig. 3.

As the composites are composed of multiple constituents (matrix, interphase and fiber), the Raman spectra of the constituents were collected separately (Fig. 3a). The Raman spectra of the SiC matrix contain two main peaks in the wavenumber range of 500~1200 cm^{-1}: transverse optical peak at ~796 cm^{-1} and longitudinal optical peak at ~973 cm^{-1} (Fig. 3b) [27,28]. The Raman spectra of the BN interphase show a sharp and strong peak at ~1365 cm^{-1}, which corresponds to the in-plane ring vibration (Fig. 3c) [29,30]. As the resolution of Raman spectroscopy is ~1 μm (larger than the thickness of the BN interphase), other peaks ascribed to the fiber and the matrix are also present in the Raman spectra of the BN interphase. The typical Raman spectra of the SiC fiber present three peaks: one sharp peak (~830 cm^{-1}) corresponding to SiC microcrystalline and two broad peaks (1330~1360 cm^{-1} and 1585~1600 cm^{-1}) corresponding to graphite phase surrounding the SiC microcrystalline (Fig. 3d) [31]. The graphite peak at larger wavenumber is called G peak, which is resulted from the vibration of carbon network plane, and has proved to be highly sensitive to the residual stress of SiC fiber [32,33]. With the temperature rising from room temperature (RT) to 1400℃, slight peak shift occurs as indicated by the dashed lines in the spectra, indicating that the residual stress of the composites experiences significant variation.

To calculate the residual stress, the peak shift ($d\lambda$) should be measured as precisely as possible. In general, $d\lambda$ can be expressed as the difference between the wavenumbers corresponding to the peak summits ($d\lambda = \lambda' - \lambda$). This may cause large measurement error when the peak shape is not symmetrical. Considering the irregular peak shape, barycenter method is used here to determine the $d\lambda$ value [34,35]. The calculation of $d\lambda$ based on barycenter method can be schematically shown in Fig. 4. Firstly, Raman peak intensity is normalized by the formula below: (see Equation 1 in the Supplementary Files)

Where I_n and I_i represent the normalized and the initial intensities of the Raman spectra, respectively. I_{min} and I_{max} are the minimum and the maximum intensities of the Raman spectra, respectively. Secondly, the

baseline intensity (I_0) of the Raman spectra is defined as: (see Equation 2 in the Supplementary Files)

Import the data of I_n and I_0 into Origin software and then a normalized peak and a horizontal baseline can be obtained, which generates two intersections (λ_1 and λ_2). Then the barycenter position (λ_b) is calculated according to the formula as below: (see Equation 3 in the Supplementary Files)

Then the peak position shift (dλ) and the residual stress (σ_r) can be obtained as follows: (see Equations 4 and 5 in the Supplementary Files)

Where and are the barycenter positions of the Raman peaks at stressed and stress-free states, respectively. C is conversion factor of Raman shift to residual stress. Characteristic peaks at 796 cm^{-1}, 1365 cm^{-1} and 1585 cm^{-1} are chosen as the calculation references for the matrix, interphase and fiber, respectively. The corresponding C values are listed in Table 1.

Table 1 Characteristic peak positions at stress-free states and conversion factors of peak shift to stress

Constituent	Characteristic peak position at stress-free state (cm^{-1})	Conversion factor C ($GPa•cm^{-1}$)
SiC matrix	796	-0.2833 [28]
BN interphase	1365	-0.2950 [36]
SiC fiber	1585	-0.1038 [31]

The peak shift (dλ) and residual stress (σ_r) at RT~1400℃ are shown in Fig. 5. Both the matrix and the fiber show positive dλ while the interphase shows negative dλ in the temperature range. This indicates the matrix and the fiber bear compressive stress while the interphase bears tensile stress. With the temperature rising from RT to 1400℃, dλ of the matrix and the fiber decreases from 4.56 cm^{-1} to 2.20 cm^{-1} and from 8.07 cm^{-1} to 5.30 cm^{-1}, respectively, while that for the interphase increases from -0.55 cm^{-1} to -0.35 cm^{-1}. Correspondingly, the residual stresses of the matrix and the fiber decrease from 1.29 GPa to 0.62 GPa and from 0.84 GPa to 0.55 GPa in compression, while that for the interphase decreases from 0.16 GPa to 0.10 GPa in tension. The thermal expansion coefficient of the interphase is ~2.7×10^{-6} $℃^{-1}$, which is much lower than the fiber (~5.0×10^{-6} $℃^{-1}$) and the matrix (~4.6×10^{-6} $℃^{-1}$). This makes the interphase in tension while both the fiber and the matrix in compression due to the mismatch of the thermal expansion coefficients. The different residual stress states of the constituents can be further confirmed by the mechanical properties of the composites, as residual stress can significantly influence the mechanical behavior by changing the stress distribution.

The mechanical response of SiC_f/SiC composites can be roughly divided into three stages. Firstly, the SiC matrix cracks when the applied stress reaches to the critical value beyond the matrix can endure. With the increase of the applied stress, the cracks in the matrix can propagate to the interphase and lead to fiber/matrix debonding. Finally, the fiber pulls out and fractures as the applied stress rises to the fracture

strength. Based on the calculation results (Fig. 5b), the matrix of the composites bears residual compressive stress, which can suppress the formation of cracks in the matrix. Meanwhile, the interphase bears residual tensile stress, which can accelerate crack propagation to the interphase and thus facilitate fiber/matrix debonding and fiber pulling-out. With the increase of temperature, fiber/matrix debonding and fiber pulling-out can be restricted due to the decreasing residual tensile stress. This leads to different fracture modes in terms of “easy” and “hard” fiber pulling-out (Fig. 6). However, the mechanical behavior of the composites should be much more complicated considering the synergistic effect of the residual stresses in the matrix and the fiber.

In order to investigate the effects of residual stress on the mechanical properties, tensile mechanical tests were performed on the as-received and heat-treated composites. The composites were heat-treated at 1000℃ and 1400℃ for 10h, respectively. Higher temperature heat treatment contributes to lower residual stress in the composites according to Fig. 5b. The tensile stress-strain curves of the composites are shown in Fig. 7 and the mechanical properties are summarized in Table 2. The tensile strength almost remains unchanged regardless of the heat-treatment, while a slight decrease can be seen in the tensile strain of heat-treated composites compared with the as-received ones. The unchanged tensile strength indicates that the decreasing residual stress has little effect on the mechanical strength. The decrease of tensile strain should be attributed to the restricted fiber/matrix debonding and fiber pulling-out caused by the lower residual tensile stress in the interphase.

Table 2 Mechanical properties of as-received and heat-treated SiC_f/SiC composites

Sample	Tensile strain (%)	Tensile strength (MPa)
As-received SiC_f/SiC	0.57±0.07	236±15
1000℃/10h	0.52±0.04	251±13
1400℃/10h	0.48±0.03	247±17

The tensile fracture surfaces of the composites (Fig. 8) confirm that the composites show different fracture modes due to the variation of residual stress. The fiber pull-outs in the heat-treated composites are a little shorter than those in the as-received samples. This is resulted from lower residual tensile stress in the interphase which restricts fiber pulling-out. Furthermore, the fractured fiber surface of the heat-treated composites is rougher than that of the as-received composites. As the residual tensile stress in the composites heat-treated at 1400℃ is much smaller than the other composites, interphase debonding and fiber pulling-out are suppressed violently. This leads to rougher fiber surface and shorter fiber pull-outs. The effects of residual stress on the mechanical properties should be very intricate considering the anisotropic structures and multiple constituents of the composite. Furthermore, the residual stress is strongly dependent on preparation methods and post-treatment conditions. Therefore, the overall understanding of residual stress in the composites still needs more researches. Nevertheless, this study promotes the research by revelation of residual stress variation in SiC_f/SiC composites and its effects on the mechanical behavior of the composites.

4. Conclusions

In this study, the residual stress of SiC_f/SiC composites was investigated using high-temperature Raman spectrometer. Because of the anisotropic structures and the multiple constituents, the composites show high residual stress and the magnitude of residual stress is closely related with temperature. With the temperature increasing from room temperature to 1400℃, the residual stress of the matrix decreases from 1.29 GPa to 0.62 GPa and the fiber from 0.84 GPa to 0.55 GPa in compression, while that of the interphase decreases from 0.16 GPa to 0.10 GPa in tension. The variation of residual stress has significant effects on the mechanical behavior of the composites. Compared with the as-received composites, the composites heat-treated at 1000℃ and 1400℃ for 10h show decreasing tensile strain. This is caused by the reduction of residual tensile stress in the interphase, which suppresses fiber/matrix debonding and fiber pulling-out. Nevertheless, the tensile strength of the composites almost remains unchanged regardless of the variation in the residual stress. This may be resulted from the synergistic effect of residual stresses in the fiber and the matrix. Although revealing the effects of residual stress on the mechanical behavior of SiC_f/SiC composites needs much more research efforts, still, this study offers new insight for residual stress variation in the composites.

Declarations

Acknowledgements

Authors appreciate the financial support of the research Grant (No. 51902328) from National Natural Science Foundation of China, the research Grant (No. 19ZR1464700) from Science and Technology Commission of Shanghai Municipality and the research Grant (No. ZDRW-CN-2017-1) from Key Program of the Chinese Academy of Sciences.

References

1. Gyekenyesi AL, Morscher GN. Damage Progression and Stress Redistribution in Notched SiC/SiC Composites. *J Mater Eng Perform* 2010, **19**: 1298-1305.
2. Mei H. Measurement and calculation of thermal residual stress in fiber reinforced ceramic matrix composites. *Compos Sci Technol* 2008, **68**: 3285-3292.
3. Ma HB, Zhang GJ, Liu HL, *et al*. Effect of WC or ZrC addition on thermal residual stresses in ZrB_2-SiC ceramics. *Mater Design* 2016, **110**: 340-345.
4. Zhou P, Jin X, Chen J, *et al*. Residual stress estimation in laminated ZrB_2-SiC ultra-high temperature ceramics with strong interfaces using X-ray diffraction and indentation techniques. *Ceram Int*. 2017, **43**: 12459-12465.
5. Watts J, Hilmas G, Fahrenholtz WG, *et al*. Stress measurements in ZrB_2-SiC composites using Raman spectroscopy and neutron diffraction. *J Eur Ceram Soc* 2010, **30**: 2165-2171.

6. Watts J, Hilmas G, Fahrenholtz WG, *et al*. Measurement of thermal residual stresses in ZrB_2-SiC composites. *J Eur Ceram Soc* 2011, **31**: 1811-1820.
7. Jannotti P, Subhash G, Zheng J, *et al*. Measurement of microscale residual stresses in multi-phase ceramic composites using Raman spectroscopy. *Acta Mater* 2017, **129**: 482-491.
8. Ghosh D, Subhash G, Orlovskaya N. Measurement of scratch-induced residual stress within SiC grains in ZrB_2-SiC composite using micro-Raman spectroscopy. *Acta Mater* 2008, **56**: 5345-5354.
9. Steen M. Tensile mastercurve of ceramic matrix composites: significance and implications for modelling. *Mat Sci Eng A-Struct* 1998, **250**: 241-248.
10. Steen M. Effect of residual stresses on the mechanical response of continuous fibre reinforced ceramic matrix composites. In: Advanced multilayered and fibre-reinforced composites, Proceedings of the NATO Advanced Research Workshop, 1997 June 2-6; Kiev, Ukraine, Netherlands; 1997, 297-309.
11. Anastassakis E, Pinczuk A, Burstein E, *et al*. Effect of static uniaxial stress on the Raman spectrum of silicon. *Solid State Commun* 1970, **8**: 133-138.
12. Wing BL, Esmonde-White F, Halloran JW, *et al*. Microstress in reaction-bonded SiC from crystallization expansion of silicon. *J Am Ceram Soc* 2016, **99**: 3705-3711.
13. John FD, Thomas EF. Analysis of Residual Stress in 6H-SiC Particles within Al_2O_3/SiC Composites through Raman Spectroscopy. *J Am Ceram Soc* 1992, **75**: 1854-1857.
14. Jin X, Sun Y, Hou C, *et al*. Investigation into cooling-rate dependent residual stresses in ZrB_2-SiC composites using improved Raman spectroscopy method. *Ceram Int* 2019, **45**: 22564-22570.
15. Yang Q, Hwang C, Khan A, *et al*. Anisotropy and residual stress in B_4C-ZrB_2 eutectic. *Mater Charact* 2019, https://doi.org/10.1016/j.matchar.2019.109797.
16. Su F, Huang P. Microscopic Mechanism of the High-Temperature Strength Behaviour of a C/SiC Composite. *Appl Compos Mater* 2019, **26**: 1059-1071.
17. Kollins K, Przybyla C, Amer MS. Residual stress measurements in melt infiltrated SiC/SiC ceramic matrix composites using Raman spectroscopy. *J Eur Ceram Soc* 2018, **38**: 2784-2791.
18. Knauf M, Przybyla C, Ritchey A, *et al*. Residual stress determination of silicon containing boron dopants in ceramic matrix composites. *J Eur Ceram Soc* 2019, **102**: 2820-2829.
19. Knauf M, Przybyla C, Ritchey A, *et al*. Measuring the effects of heat treatment on SiC/SiC ceramic matrix composites using Raman spectroscopy. *J Eur Ceram Soc* 2019, https://doi.org/10.1111/jace.16724.
20. Dong S, Katoh Y, Kohyama A. Preparation of SiC/SiC Composites by Hot Pressing, Using Tyranno-SA Fiber as Reinforcement. *J Am Ceram Soc* 2003, **86**: 26-32.
21. Amer MS. Raman Spectroscopy, Fullerenes, and Nanotechnology. Royal Society of Chemistry, Cambridge, UK, 2010.
22. Gouadec G, Karlin S, Wu J, *et al*. Physical chemistry and mechanical imaging of ceramic-fibre-reinforced ceramic- or metal-matrix composites. *Compos Sci Technol* 2001, **61**: 383-388.

23. Wang H, Gao S, Peng S, *et al*. KD-S SiC_f/SiC composites with BN interface fabricated by polymer infiltration and pyrolysis process. *J Adv Ceram* 2018, **7**: 169-177.
24. Chai Y, Zhou X, Zhang H. Effect of oxidation treatment on KD-II SiC fiber-reinforced SiC composites. *Ceram Int* 2017, **43**: 9934-9940.
25. Yu S, Chen Z, Wang Y, *et al*. Effect of fabric structure on the permeability and regeneration ability of porous SiC_f/SiC composite prepared by CVI. *Ceram Int* 2019, **45**: 11564-11570.
26. Tao P, Wang Y. Improved thermal conductivity of silicon carbide fibers-reinforced silicon carbide matrix composites by chemical vapor infiltration method. *Ceram Int* 2019, **45**: 2207-2212.
27. Fist N, Dinan J, Stadelmann R, *et al*. In situ three point bending device for measurements of vibrational response of ceramics under stress by microRaman spectroscopy. *Adv Appl Ceram* 2012, **111**: 433-439.
28. Zhu W, Zhu J, Nishino S, *et al*. Spatially resolved Raman spectroscopy evaluation of residual stresses in 3C-SiC layer deposited on Si substrates with different crystallographic orientations. *Appl Surf Sci* 2006, **252**: 2346-2354.
29. ul Ahmad A, Liang H, Ali S, *et al*. Cheap, reliable, reusable, thermally and chemically stable fluorinated hexagonal boron nitride nanosheets coated Au nanoparticles substrate for surface enhanced Raman spectroscopy. *Sensor Actuat B-Chem* 2020, https://doi.org/10.1016/j.snb.2019.127394.
30. Du M, Li X, Wang A, *et al*. One-Step Exfoliation and Fluorination of Boron Nitride Nanosheets and a Study of Their Magnetic Properties. *Angew Chem Int Edit* 2014, **126**: 3719-3723.
31. Niu X, Zhang H, Pei Z, *et al*. Measurement of interfacial residual stress in SiC fiber reinforced Ni-Cr-Al alloy composites by Raman spectroscopy. *J Mater Sci Technol* 2019, **35**: 88-93.
32. Colomban P, Gouadec G, Mathez J, *et al*. Raman stress measurement in opaque industrial C_f/epoxy composites submitted to tensile strain. *Compos Part A-Appl S* 2006, **37**: 646-651.
33. Young R, Eichhorn S. Deformation mechanisms in polymer fibres and nanocomposites. *Polymer* 2007, **48**: 2-18.
34. Zhang W, Li Z, Baxter G, *et al*. Stress- and Temperature-Dependent Wideband Fluorescence of a Phosphor Composite for Sensing Applications. *Exp Mech* 2017, **57**: 57-63.
35. Zhang W, Wang G, Baxter G, *et al*. Methods for Broadband Spectral Analysis: Intrinsic Fluorescence Temperature Sensing as an Example. *Appl Spectrosc* 2016, **71**: 1256-1262.
36. Erasmus R, Comins J, Fish M, *et al*. Raman spectroscopy as a technique to characterize stress in diamond and cubic boron nitride. AIP Conference Proceedings. 2000, **509**: 1637-1644.

Figures

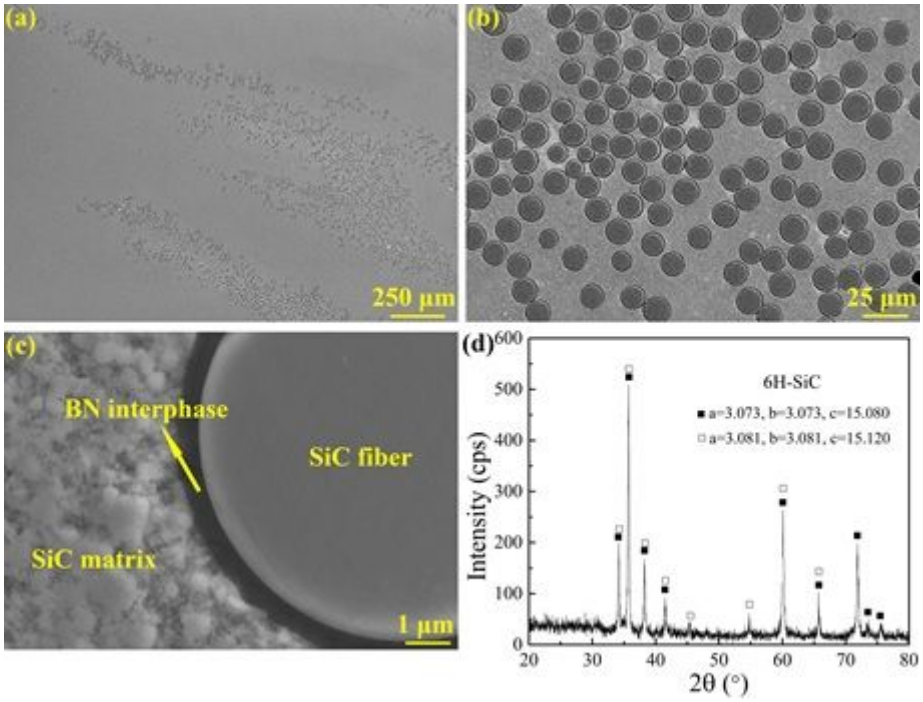

Figure 1

SEM images of the cross-sectional SiCf/SiC composites and (d) XRD patterns of the composites.

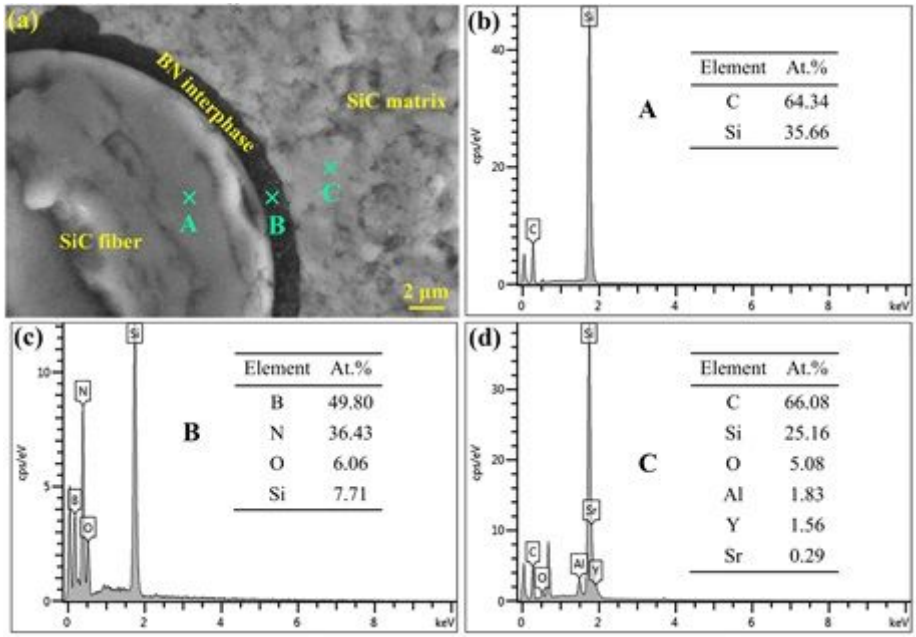

Figure 2

Energy dispersive spectra of the as-received SiCf/SiC composites.

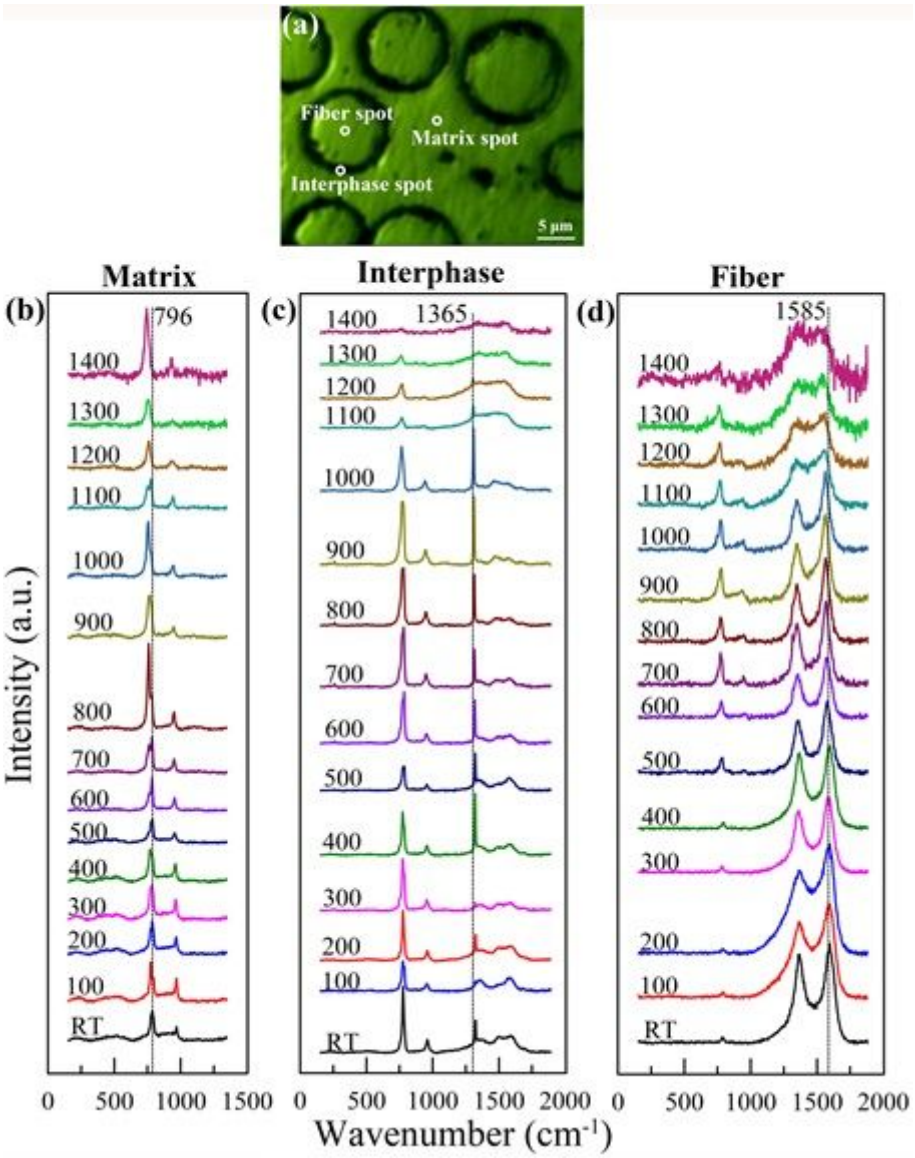

Figure 3

Selected spots for Raman spectrum detection and the corresponding Raman spectra (b-d) at RT~1400℃.

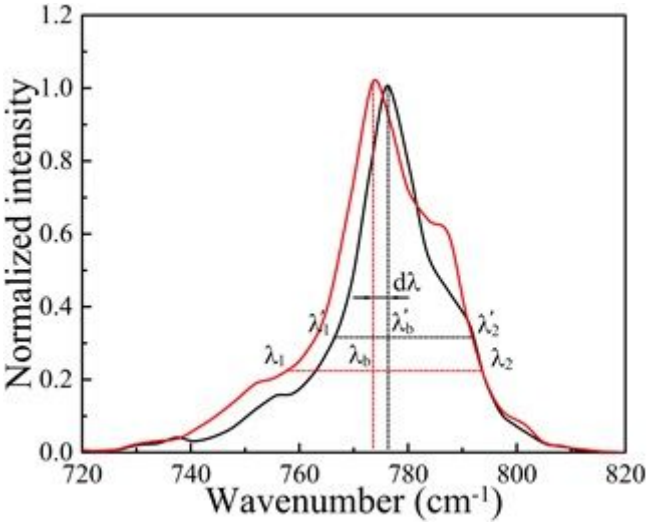

Figure 4

Schematic of calibrating peak position shift based on barycenter method.

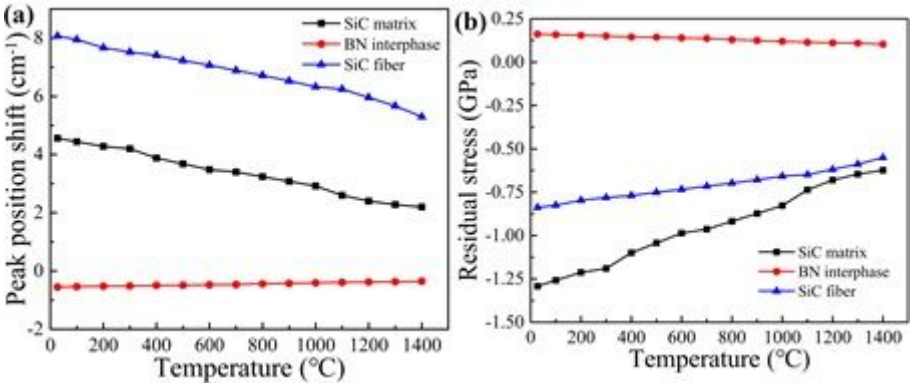

Figure 5

(a) Raman peak position shift and (b) residual stress as a function of temperature.

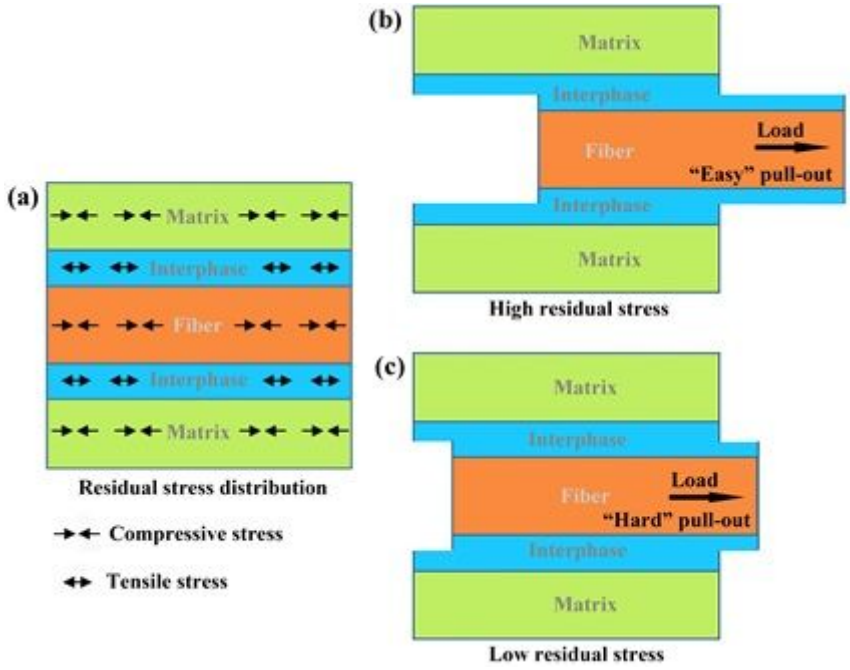

Figure 6

Schematic of (a) residual stress distribution in SiCf/SiC and (b-c) mechanical behaviors under low and high residual stresses.

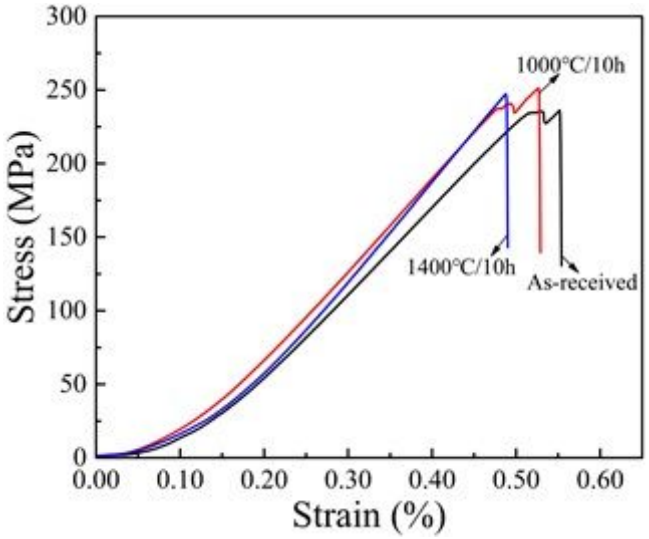

Figure 7

Tensile stress-strain curves of as-received and heat-treated SiCf/SiC composites.

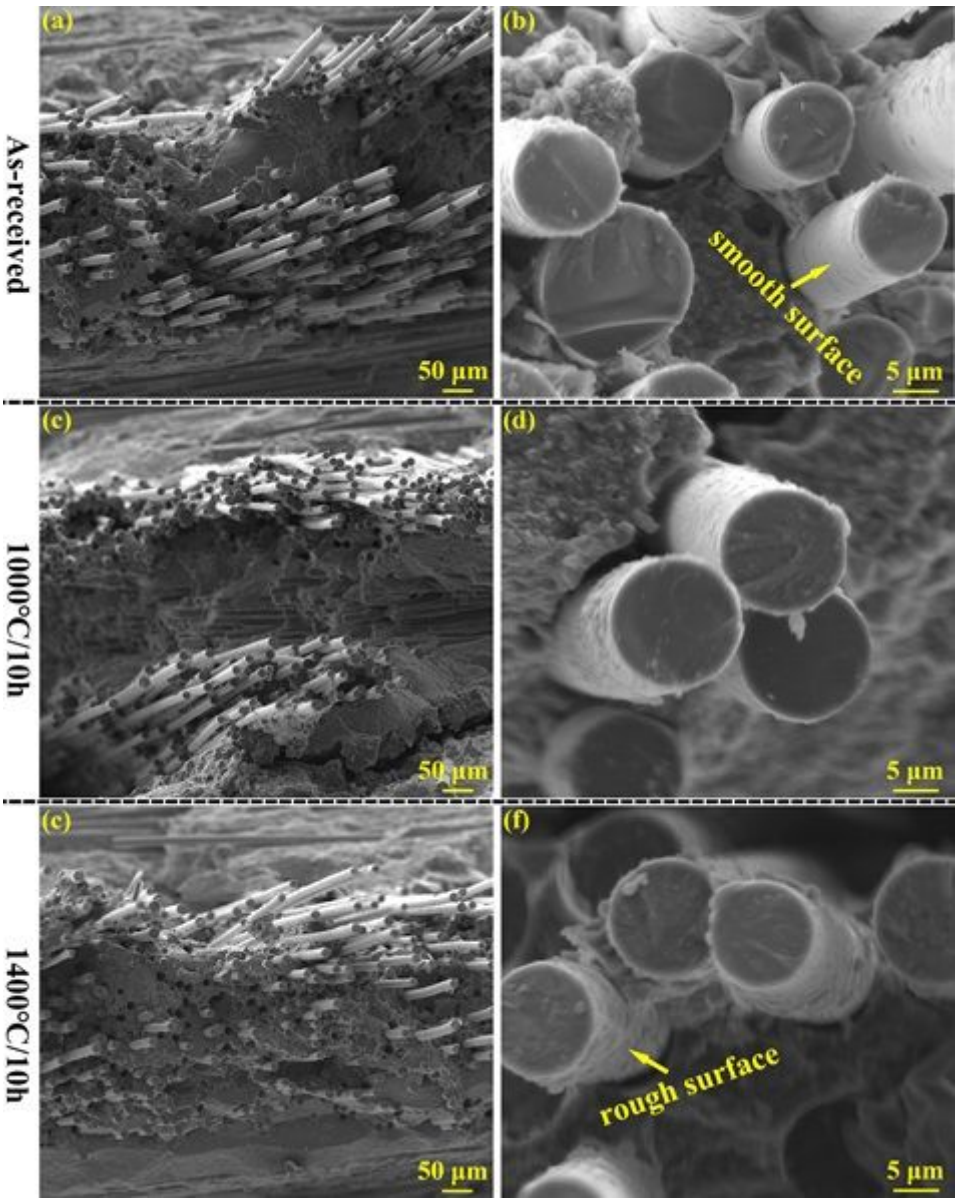

Figure 8

SEM images of the SiCf/SiC composites fracture surfaces: as-received (a-b) and heat-treated at 1000℃ (c-d) and 1400℃ (e-f) for 10h.

Supplementary Files

This is a list of supplementary files associated with this preprint. Click to download.

- Equations.pdf